Indazole versus indole-based cationic merocyanines with red shifted in-cellulo emission for selective mitochondria imaging

Margot Boujut, Arnaud Chevalier, Damien Schapman, Magalie Bénard, Ludovic Galas, Thibault Gallavardin, Xavier Franck

Indazole *versus* indole-based cationic merocyanines with red shifted *in-cellulo* emission for selective mitochondria imaging.

Margot Boujut,[a] Arnaud Chevalier,[a] Damien Schapman,[b] Magalie Bénard,[b] Ludovic Galas,[b] Thibault Gallavardin,*[a] Xavier Franck.*[a]

a Normandie Univ, CNRS, INSA Rouen, UNIROUEN, COBRA, 76000 Rouen, France

E-mail: margot.boujut@etu.univ-rouen.fr

Arnaud.chevalier@cnrs.fr

thibault.gallavardin@univ-rouen.fr

xavier.franck@insa-rouen.fr

b Normandie Univ, Inserm, UNIROUEN, PRIMACEN, 76000 Rouen, France

E-mail: damien.schapman@univ-rouen.fr

magalie.benard@univ-rouen.fr

ludovic.galas@univ-rouen.fr

*co-last authors

Key words: Fluorophore; Cellular biology; Indazole; Cationic merocyanine dyes; Mitochondria;

Abstract

Selective fluorophores are seminal for the development of fluorescent cell imaging allowing the simultaneous monitoring of several biological parameters. Mitochondria are one of the main targets of optical microscopy as their dynamics are related to many biological events. One of the best strategy to target them, is to design cationic dyes which accumulate preferentially in their membranes due to their high electrochemical potential. In this work, indazole scaffold was explored to build new cationic merocyanine dyes and compared with indole scaffold. This nitrogen heteroaromatic structure is still very uncommon in dyes chemistry; therefore, a lot has to be discovered about the effects of pH, solvent polarity and methylation in cyclic nitrogen on their optical properties. Finally, fluorescent imaging revealed that a red shift occurred in the emission of these molecules inside the mitochondria.

1 Introduction

Mitochondria are one of the main targets of fluorescent bioimaging because their dynamic is related to numerous cellular processes and dysfunctions [1-3]; allowing evaluation of cells behavior. Cationic hydrophobic molecules are reported to accumulate preferentially in mitochondria, [4,5], therefore, cationic dyes are common in cell microscopy for their selective fluorescent imaging [6-24]. Indeed, their selectivity arise from the high membrane potential of this organelle, particularly in cancer cells [25,26], which retains lipophilic cations. This phenomenon was also exploited in photodynamic therapy to localize ROS generation inside tumor cells mitochondria [27-30]. This class of molecules also gave rise to the development of drugs known as “delocalized lipophilic cations” which showed cell toxicity by perturbing mitochondria membrane potential [31-33].

Merocyanine dyes are of common use in fluorescence imaging thanks to their high brightness in visible range and near infrared and their ability to sense their environment in response of several external stimuli such as polarity, H-bonding and viscosity [34-37]. These chromophores are constituted by an electron-donating group and an electron-withdrawing group linked by a polymethine chain featuring

an odd number of atoms. This arrangement provides them either a push-pull character making them good polarity probes or a cyanine character resulting in red shifted spectra. The balance between these two behaviors depends of the strength of their polarizing groups and of the polarization effect of their environment. Whereas indole is a classical electron-donating group in merocyanines [33,38], in this study, we chose to replace indole by indazole and to study the effect of this substitution. Indeed, indazole scaffold is drawing increasing attention as a key fragment for the conception of new drugs, as it is a bioisostere of indoles commonly found in bio-molecules. Replacing indole by indazole can be advantageous to tune the pharmacological profile and the affinity of a drug. Indeed, compared to indole, 1-*H*-indazole can interact more strongly with proteins thanks to its two successive nitrogen atoms able to create donor and acceptor hydrogen bonds [39-44]. Indazole scaffold has not yet been extensively exploited in chromophores design, consequently, little is known about its optical properties. On one hand, indazole is a less powerful electron-donating group than indole, but in the other hand, it should be more impacted by pH due to its more acid hydrogen. Moreover, nitrogen-containing aromatic compounds can feature very diverse optical properties as they can be used as electron-rich groups such as indoles or pyrroles, or as electron-withdrawing groups such as pyridine, pyridinium, quinoxalines. Nitrogen containing aromatic heterocycles can also favor intersystem crossing, generating triplet states though n-π* orbitals population, leading to the development of photosensitizers [45]. On the other hand, nitrogen atom can act as hydrogen bond acceptor or donor modulating electron density along the unsaturated chain, making this class of compounds interesting to probe biological environment [46].

For those reasons, we turned our attention to the synthesis of indazole-based cationic merocyanine chromophores **1**, **2** and **3** that were designed with an indazole ring endowing the role of electron-donating group and an indolinium moiety as a charged electron-accepting group to promote mitochondria targeting (Fig. 1). Indole analogues **4** and **5** were also synthetized to provide a comparison.

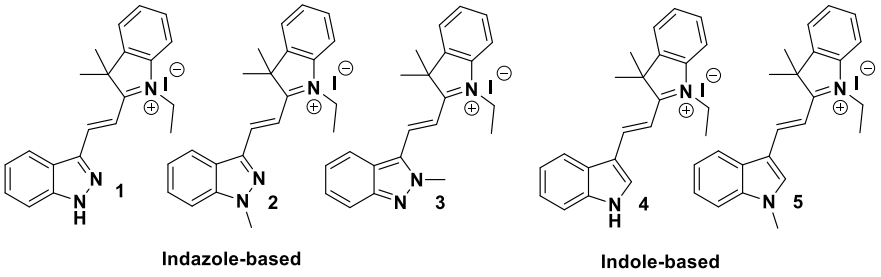

Fig. 1. Structures of indazole and indole merocyanines.

Indazole merocyanines are expected to behave similarly to indole merocyanines, but with absorption and emission spectra slightly blue-shifted because indazoles are less electron rich. In the other hand, the presence of an acidic proton in the indazole aromatic ring (pKa≈14 [47] instead of pKa≈17 for indole in water) may generate interesting probing properties because this proton can be involved in hydrogen bonds with biomolecules (Fig. S1). Finally, it can be deprotonated making indazole a powerful electron-donating group in the same way as the phenol-related phenolate. In this work 1, or 2-methyl-1*H*-indazole derivatives **2** and **3**, respectively, were synthesized as points of comparison to better understand the impact of tautomerism and deprotonation on the optical properties of these merocyanines.

2 Results and discussion

2.1 synthesis

1 was readily prepared in two steps, starting from indole **12** (Scheme 1), the first reaction being a nitrosation providing in one step indazole-3-carboxaldehyde **7**; this transformation was achieved in excellent yield according to our previously described protocol [48]. Then a Knoevenagel condensation was performed using 1-Ethyl-2,3,3-trimethyl-3*H*-indolium iodide **6** as the nucleophile to give the cationic dye **1** with 64% yield.

N-methylated products **8** and **9** were obtained jointly, as a separable mixture, by methylation of **7** with methyl iodide and a weak base at 80 °C. This relatively high temperature promotes the formation of a small amount of 2-methyl-1*H*-indazole-3-carbaldehyde **9** (13%) along with 1-methyl-1*H*-indazole-3-carbaldehyde **8** as the major product (58%).[49] Then, these latter products were reacted with **6** in the presence of piperidine to provide N-methylated dyes **2** and **3** in moderate 44% and 66% yields, respectively. Indoles **4** and **5** were prepared according the same protocol starting from commercial indoles **10** and **11.**

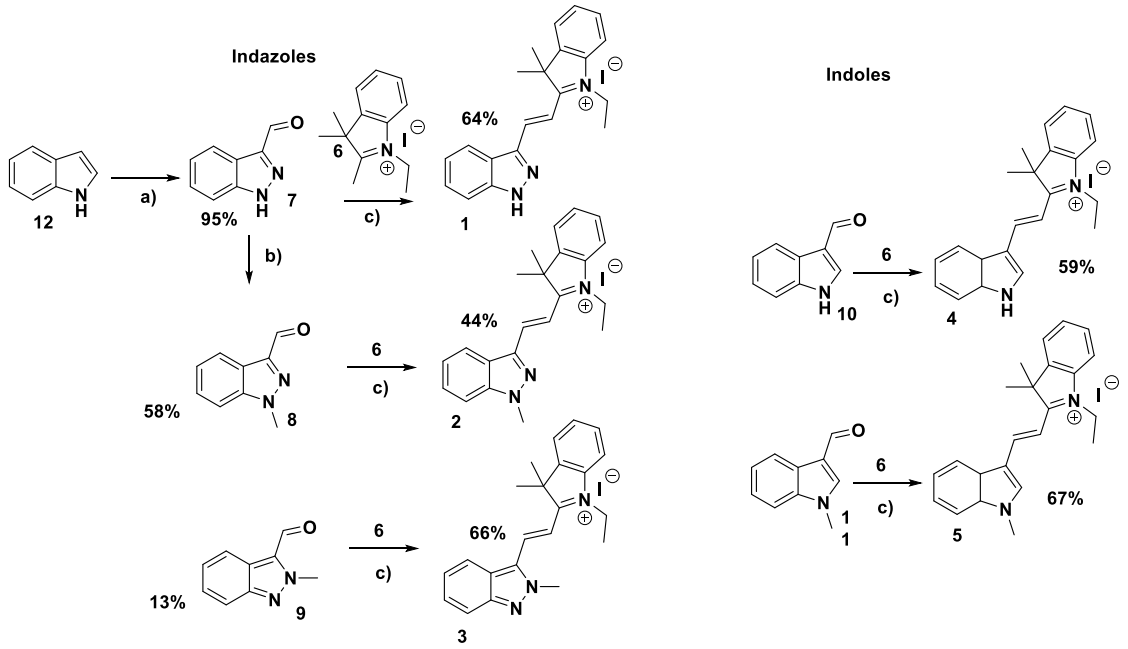

Scheme 1. Synthesis of cationic merocyanine dyes **1**-**5**. a) $NaNO_2$, DMF, H_2O, HCl, 0 °C then rt, 3h; b) MeI, K_2CO_3, MeCN, 80 °C, 16h; c) piperidine (cat), MeCN, 80 °C 16h.

2.2 Optical properties

Absorption

Absorption of **1** was studied in various solvents (Fig. 2), the first results showed the presence of two distinct absorption bands, one with maximum around 450 nm and the other around 550 nm corresponding to two distinct species. Peculiarly, the results were non-reproducible, depending on solvents batches; the balance between these two bands being variable disclosing the fact that the pKa of **1** is likely to be very close to the neutrality. Therefore, spectroscopic studies were performed after addition of acetic acid, triethylamine or sodium hydrogenocarbonate in water (0.1% in weight) causing a total displacement of the equilibrium toward protonated or deprotonated form demonstrating that no tautomerism was involved in this phenomenon.

In acidic medium, **1** presents a negative absorption solvatochromism in accordance to the classical behavior of charged compounds; the spectral shape is large corresponding to the charge transfer of a push-pull chromophore. After addition of base, a 100 nm red shift is observed and the shape of the absorption band evolves to become more “cyanin-like”, i.e. a red shifted sharper band. On the other hand, indole analogue **4** is less sensitive to pH variation. Indeed, in “pure solvent”, only the protonated form is observed, and addition of acid (acetic acid) or base (trimethylamine) do not change the spectra (Fig. 2). The absorption maximum of indole derivative **4** is red shifted (460-490 nm) by comparison with protonated indazole **1** (430-460 nm), this demonstrates that, as anticipated, indole is a stronger electron-donating group. However, indazole compound **1** is more red shifted when deprotonated (515-520 nm). This observation suggests that indazole can be classified as less electro-donating when protonated than indole, but a stronger electro-donating group after deprotonation.

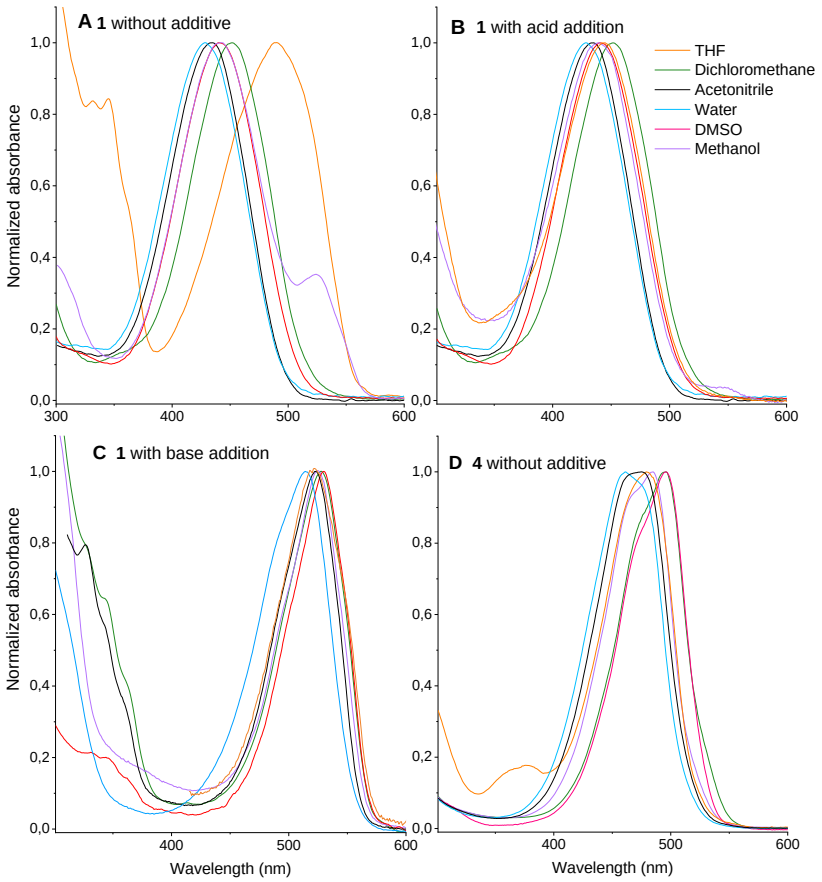

124

125 Fig. 2. Absorption solvatochromism of **1** at 21 °C in pure solvent (A) and effect of acid (B) or base
126 addition (C), and comparison with **4** in pure solvent (D). Water (blue), acetonitrile (black), DMSO
127 (red), methanol (mauve), dichloromethane (green), THF (orange).

128

129 The pKa of **1** was determined in PBS by carrying out absorption spectra in a pH range from 6.89 to
130 10.59 monitored by small addition of K_2CO_3. The presence of an isobestic point at 468 nm
131 demonstrated the progressive deprotonotation of indazole **1** (Fig. 3). The absorption maximum in
132 function pH was plotted (Fig. 3) and Henderson-Hasselbach equation (equation S1) was used to
133 calculate the pKa, it was found to be close to 9.0 (Fig. 3). By comparison, the pKa of non-functionalized
134 indazole was reported to be 13.86 in water [47]. This pKa value is in accordance with the pH effect

observed in organic solvents in which deprotonated form is more stabilized than the ionic protonated form.

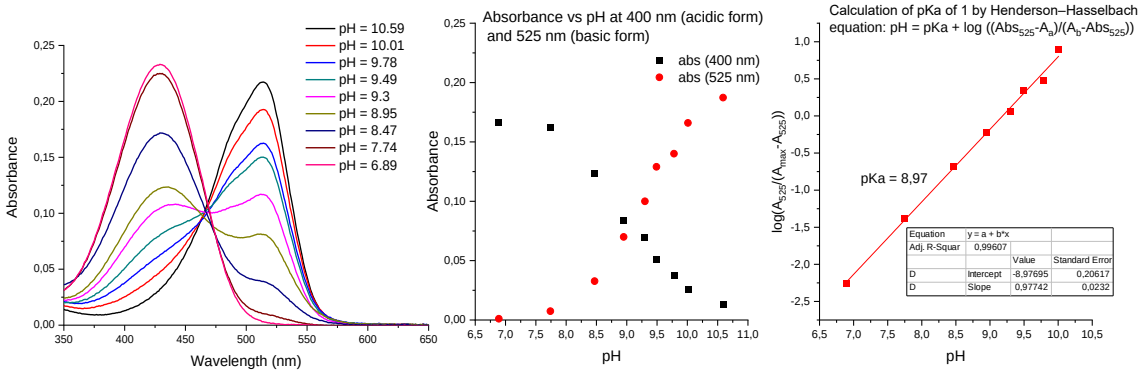

Fig. 3. Absorption of **1** in function of pH in PBS solutions and calculation of pKa by Henderson-Hasselbach equation at 525 nm: the ground state pKa of **1** can be read at y-intercept: 8.97 in PBS.

Fluorescence

The profile of the fluorescence of merocyanine **1** was then studied in the same solvents (Fig. 4). In acidic medium, the fluorescence quantum yield is very low (0.02) in dichloromethane and no solvatochromism was observed (Fig. 4). In the basic form, fluorescence quantum yield of **1** was still very low (0.03) in dichloromethane, but the emission spectral shape was highly modified, it became more “cyanin like” i.e. with an emission band shifted to higher wavelengths with a shoulder in the red side and the solvatochromism was very weak. Unexpectedly, the fluorescence wavelength of indole **4** is very close to the one of protonated indazole **1** with maximum comprised between 525 nm and 550 nm and the solvatochromism is negligible. As its absorption is red-shifted by comparison to **1**, the stokes shift of **4** is very small (1633 cm^{-1}) indicating that the polarity of the fundamental and the emitting states are very close.

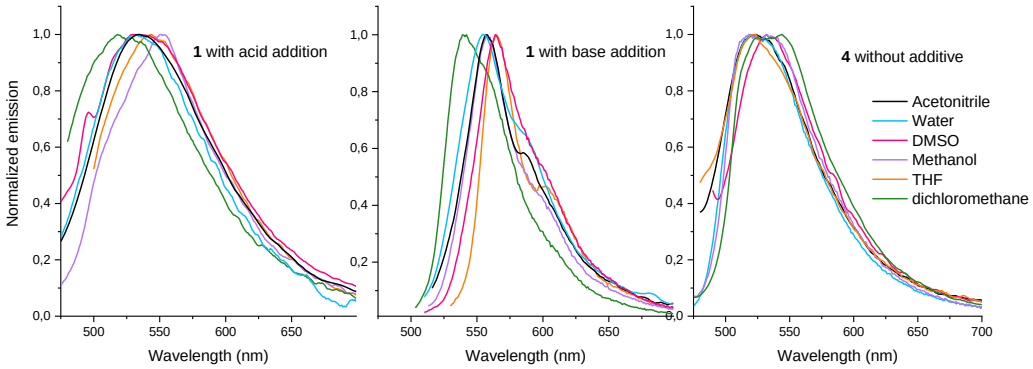

Fig. 4. Fluorescence solvatochromism of **1** at 21 °C with addition of acid (left), or base (right). Water (blue), acetonitrile (black), DMSO (red), methanol (mauve), dichloromethane (green), THF (orange).

In the case of indazole **1**, in neutral medium (not shown), the fluorescence signals of both basic and acidic forms were observed in similar ratio than absorption, meaning that no excited state deprotonation occurred. The coexistence of the emissions of both forms suggests that emission is faster than proton exchange, and therefore that the fluorescent lifetime of this molecule is likely to be very short. Indeed, fluorescence decays were measured and proved to be short in dichloromethane with a main component below 300 ps for both protonated and deprotonated forms (Fig. S2). Very short fluorescence lifetimes were also measured for indole **4** below 300 ps. These results are in accordance with previous measurements in structurally close compounds aztragon orange-R [50] and basic orange 21 [51] bearing indoles as donors. This low fluorescence might be related to the generation dark "phantom" excited states in which fast deexcitation occurs due to the formation of twisted excited states [52]. These results suggested that the fluorescence efficiency of these molecules can be modulated by solvent viscosity.

Comparison with methylated compounds

The optical properties of methylated compounds **2** **3,** and **5** were then studied in dichloromethane (Fig. 5). 1-methylated indazole **2** featured similar spectra shape to **1** but absorbed at 460 nm (vs 450

nm) and emitted at higher wavelength (551 nm vs 533 nm). This bathochromic shift was ascribed to the inductive effect of the methyl group making indazole a stronger donor, at a lesser extent, the same phenomenon was observed in absorption with indole **5** in comparison with indole **4** (5 nm red-shift). This demonstrates that the proton is localized on nitrogen in position 1 in indazole **1**. In comparison, 2-methylated indazole **3** featured very different spectral shapes with absorption and emission red shifted, and a low Stokes shift (2020 cm^{-1} vs ≈ 3500 cm^{-1}); this behavior suggested that the molecule has more "cyanine" character. This phenomenon is related to the theoretical modelling done by Catalan, showing that 2-methylation of indazoles changes its electronic density making it more "quinoid" like, and less aromatic [47]. This loss of aromaticity in molecule **3** favors electron delocalization explaining it's "cyanine" character [53]. The effect of the methylation of indole is very weak as the absorption and emission of **5** are very close to those of **4.** Indole compounds feature higher absorption wavelength than **1** and **2** and their Stokes shifts are very low (1600 cm^{-1} and 1200 cm^{-1} respectively for **4** and **5**), in addition, their absorption and emission band are symmetrical which is very typical of cyanine fluorophores. It is noticeable that the most red-shifted fluorophore in dichloromethane is indazole **3**, methylation of nitrogen in position 2 favors electrons delocalization by decreasing the aromaticity of indazole.

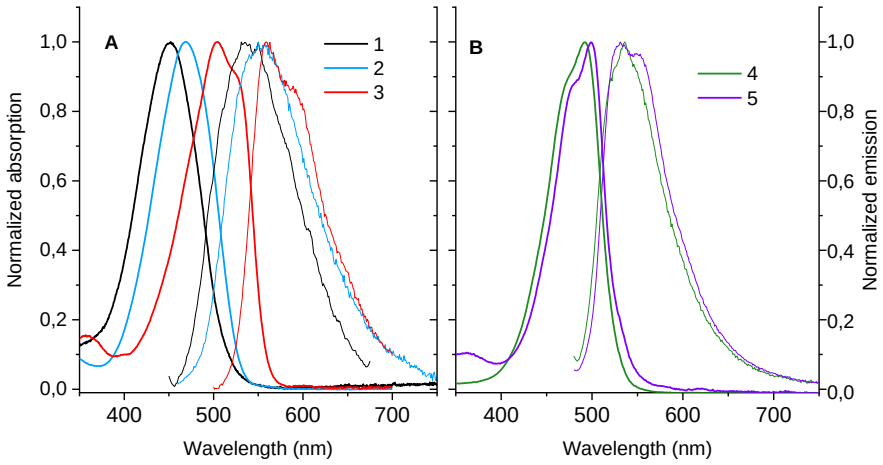

Fig. 5. Absorption and emission of (left) **1** (black), **2** (blue) and **3** (red) and (right) **4** (green) and **5** (violet) in dichloromethane at 21 °C.

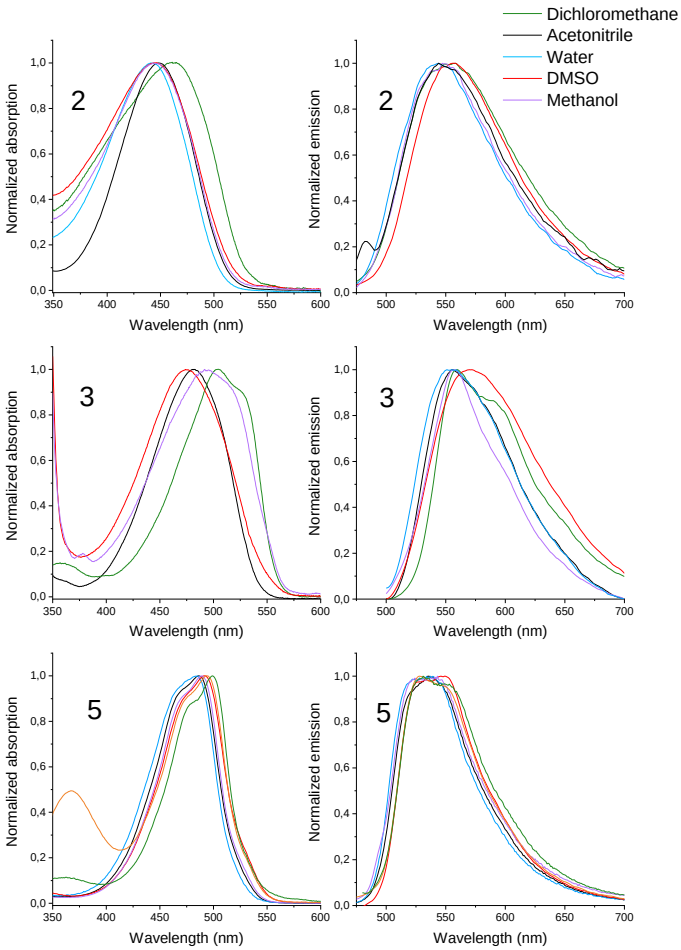

Fig. 6. Absorption and emission at 21°C of methylated compounds in water (blue), acetonitrile (black), DMSO (red), methanol (mauve), dichloromethane (green), THF (orange).

2.3 Viscosity response

The viscosity dependence of the fluorescence was measured by varying the composition of an ethylene glycol/glycerol mixture. This mixture was chosen to keep constant the solvent polarity during all the experiment. The fluorescence ln(F) as a function of viscosity ln(η) was plotted (Fig. 7) and (Table 1), the slope showed that dependence of the fluorescence of **1** upon viscosity (0,62) is high, slightly lower

than those measured with best commercial viscosity probes PicoGreen® (0,72) and SYBR Green I (0,75) [54]. 1-methylated indazole **2** showed the same dependence (0.60), while 2-Methylated indazole **3** featured a lower fluorescence response (0,45). By comparison, indoles featured slightly less fluorescence dependence upon viscosity with slopes respectively at 0.56 for **4** and 0.47 for **5**. This fluorescence dependence upon viscosity was high enough to make these compounds promising for viscosity imaging in mitochondria [55].

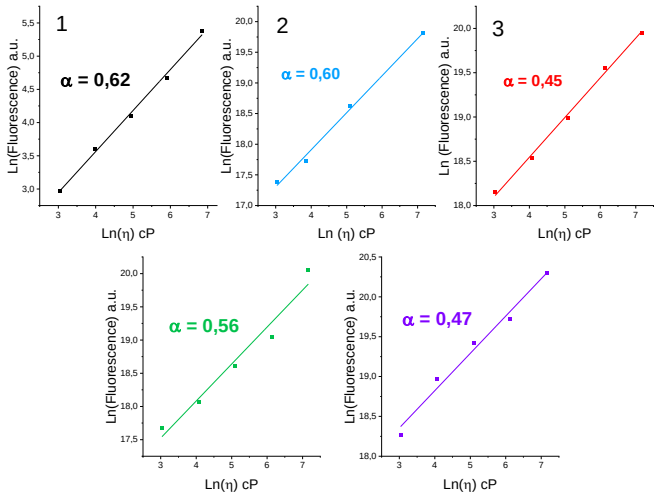

Fig. 7. Fluorescence signal (ln(F)) of **1**-**5** in function of viscosity (ln(η)) in ethylene glycol/glycerol mixtures.

	ε^a	λ_{abs} (nm)	λ_{em} (nm)	Stokes shift[b]	ϕF^c	viscosity slope
1	34 000	450	533	3460	0.02	0.62
2	23000	460	551	3590	0.01	0.60
3	30 000	503	560	2020	0.02	0.44
4	46000	492	535	1633	0.01	0.56
5	44000	499	532	1243	0.01	0.47

Table 1. Spectroscopic data of **1**-**5** in dichloromethane at 21 °C. [a] molar extinction given in ($mol^{-1}.L.cm^{-1}$),[b] Stokes shift given in cm^{-1}, [c] fluorescence quantum ϕF yield was measured using coumarine 153 (ϕF =0.54) in ethanol as reference [56].

3 Fluorescence imaging

3.1 Fluorescence images

Fluorescence images were recorded in tumoral PC12 cells. At high magnification (63x objective, NA 1.4), xyz acquisitions revealed that incubation with **1**, **2** or **3** (10^{-6} M, 45 min) induced a combination of numerous moderately stained filamentous structures and sparse hot spots in the entire cytoplasm (Fig. 8 A, D, G). Intensively fluorescent spots were either linked to filamentous structures or isolated. In contrast, plasma and nuclear membranes were devoid of labeling (Fig. 8 A, D, G).

In addition, double-labeling experiments indicated that indazole based-merocyanines **1**, **2** or **3** co-localized strongly with mitochondria labeling (MitoTracker™ Green) both for filamentous and spot-shape structures (Fig. 8) (Pearson correlation coefficients: 0.827, 0.838 and 0.756 respectively for **1**, **2** and **3**). The fluorescence localization in cells of indole derivatives **4** and **5** was also studied; co-localization was implemented with MitoTracker™ Red since indole compounds emission overlapped with MitoTracker™ green emission. Unexpectedly, these two molecules did not localize in the same cell compartment, **4** was not able to reach mitochondria and featured a liposomal localization, while **5** localized selectively in mitochondria similarly to indazole compounds.

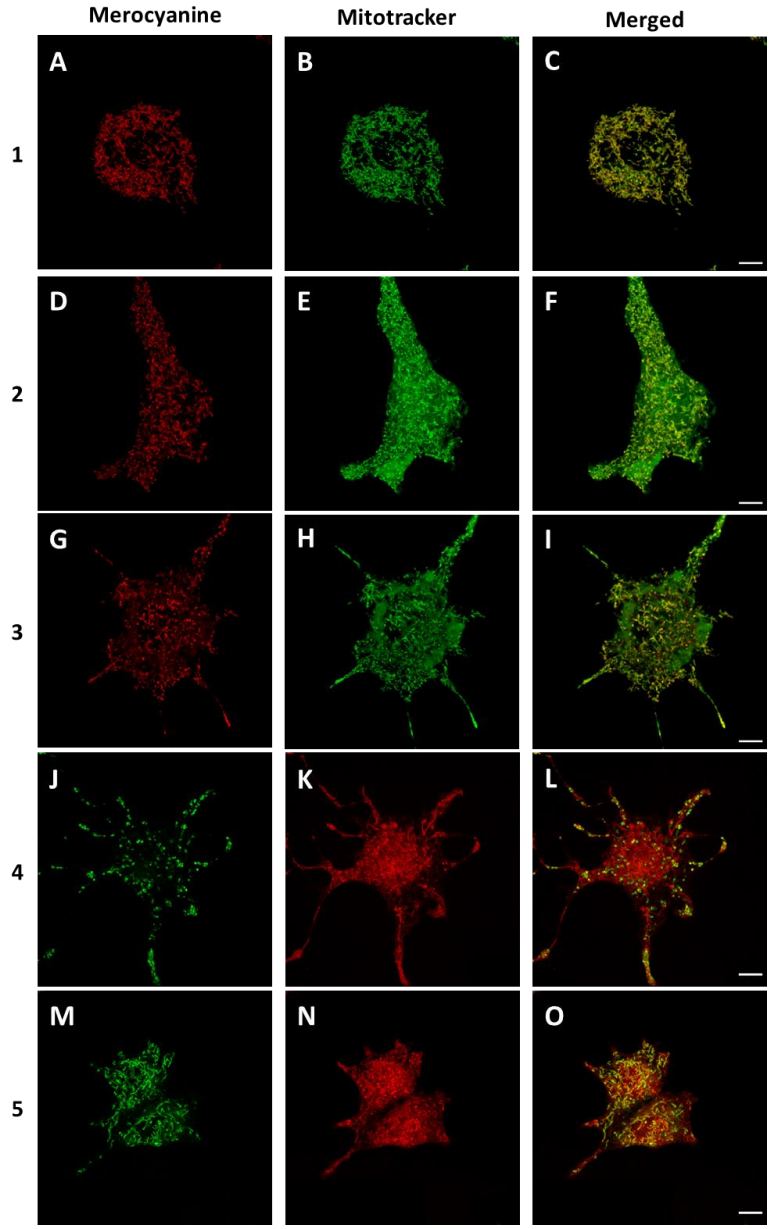

230

231 Fig. 8. Subcellular staining of living PC12 cells with **1** - **5** through confocal microscopy. Single staining
232 (Left). Single staining for the mitochondria marker MitoTracker™ Green (panels B, E, H) and
233 MitoTracker™ Red (Panels K, N). Double staining with **1**, **2** or **3** and MitoTracker™ Green (panels C, F,
234 I) and **4** or **5** with MitoTracker™ Red (Panels L, O). Scale bar 10 µm

235

236 **3.2 cytotoxicity**

A fluorescent membrane integrity test with the NucGreen™ reagent indicated that 1- or 24-hrs incubation with **1**, **2** or **3** (10^{-6}M) did not alter viability of PC12 cells suggesting that merocyanine compounds were not cytotoxic at this concentration (Fig. 9). Indoles cytotoxicity was also studied and similar results were obtained (SI Fig. S5).

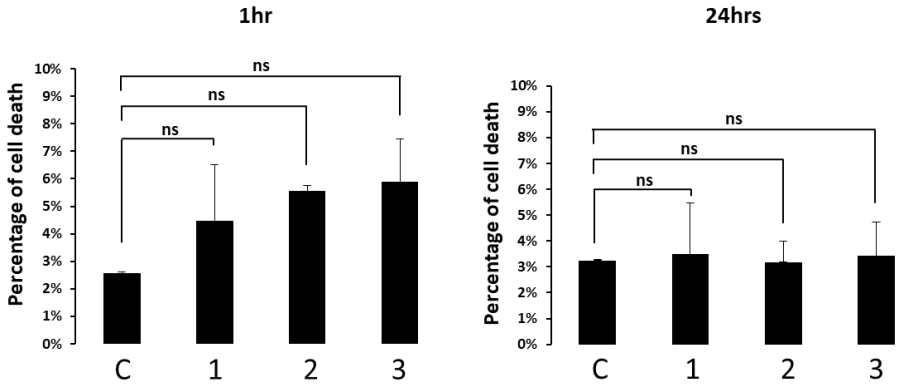

Fig. 9. Effect of merocyanine compounds (10^{-6} M) on cell viability. Measurement of the cytotoxic effect on PC12 cells after exposure with **1**, **2** or **3** during 1 hr or 24 hrs through fluorescent membrane integrity test. Each value represents the mean of the percentage of dead cell (± sem) on at least 150 cells. n.s., no statistical significance versus control.

3.3 *In cellulo* spectra

In cellulo excitation and emission spectra were recorded for each compound (Fig. 10). Surprisingly, for indazoles compounds, they were very distinct from spectra in cuvettes; they both featured very similar spectra with an excitation maximum at 540 nm and fluorescence maximum at 580 nm corresponding to a 20-40 nm red shift by comparison with fluorescence emission in pure solvent. In the case of **1** the red shift might be the result of a deprotonation inside of mitochondria, however, excitation and emission are a little bit more shifted than previously observed in basic medium (see Fig. 4). Moreover, non-deprotonable **2** and **3** featured the same excitation and emission wavelengths as **1** indicating that this fluorescence wavelength shift does not originate from deprotonation.

In cellulo emissions of indole compounds **4** and **5** were also red shifted with a maximum at 550-560 nm in comparison with water and organic solvent (530-540 nm) (Fig. 10), but their excitation spectra matched their absorbance measured in cuvette. These red shifts are clearly smaller than those of indazole compounds, resulting that, *in cellulo*, indazole compounds are more red-shifted than indoles. This behavior can be only explained by an uncommon effect affecting the optical properties of indazoles, which does not occur with indoles.

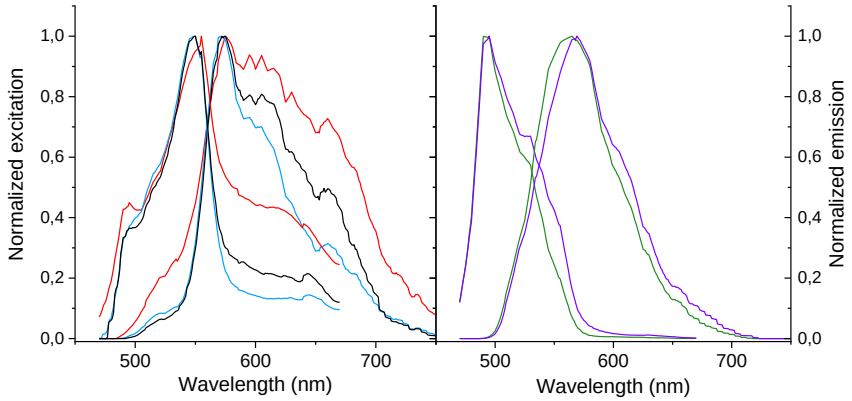

Fig. 10. *In cellulo* and excitation and emission spectra of indazoles (left) **1** (black), **2** (blue), **3** (red) andand indoles (right): **4** (green), **5** (violet).

Merocyanine color change can be induced by chemical reactions, especially, indolinium group is prone to photooxidation [57] or can suffer from nucleophilic addition of hydroxide ion [58,59] or of cyanide ion even in mild conditions [60-66]. However these reactions lead to blue shifts in absorption and emission due to conjugation breaking. Red shift was described in the case of aggregate formation, particularly J-aggregates; this phenomenon was first observed in mitochondria tagged with JC-1 cyanine dye [67]. Indeed, in the presence of a surfactant or with increasing ionic strength, many cyanines form monolayer of J-aggregates [68,69]. This phenomenon gives rise to a red shifted very sharp absorption and emission bands featuring a very weak Stokes shift resulting from cooperative

intermolecular connection of electronic density. It had been used to probe mitochondria membrane potential since more polarized mitochondrial membranes accumulate more lipophilic cationic dyes.[70]

To challenge this hypothesis, the formation of aggregates was probed by adding an aqueous saturated solution of NaCl to a water solution of **1**, **2** or **3** (final dye concentration 5 $mg.ml^{-1}$ in 3M NaCl) inside of quartz capillaries. Under UV lamp exposition, no visible fluorescence appeared in pure water while the NaCl solution became orange (Fig. 11). The fluorescence band (excitation 520 nm) was recorded with an integrating sphere in both media and a stunning exaltation was observed with all compounds (Fig. 11). The fluorescence quantum yields (QY) of molecules **1**, **2** and **3** measured with an integrating sphere reaffirmed this exaltation (Fig. 11), with molecule **1** going from fluorescence quantum yield QY = 0.001 in pure water to QY= 0.052 in NaCl solution, molecule **2** from QY= 0.007 to QY = 0.125. On the other hand, the fluorescence quantum yield change was less pronounced with molecule **3** (from QY=0.01 to QY=0.025) (Fig. 11). It is worth noting that these molecules were only partly aggregated, and a large amount remained soluble, leading to light absorption by free molecules and thus to fluorescence quantum yield underestimation; this effect was more prominent with molecule **3** because the absorption of free molecule is the most red-shifted. In order to avoid this excitation filter effect, using more diluted solutions was tested (final dye concentration 0,3 $mg.ml^{-1}$) but no or not enough aggregation occurred in order to detect aggregates emission. In our experiments, the full width at half maximum (FWHM) of the emissions remained quite large in comparison of what is commonly observed when J-aggregates are formed in surfactant monolayers. This is probably because the arrangement of the aggregates was not well ordered enough, and that a mixture of several aggregation patterns was obtained leading to larger emission bands. Moreover, the measurement of the absorption of these aggregates was not successful as there was not a distinct red-shifted absorption band, probably because only a very small part of aggregated compounds features a J-aggregate structure. As these merocyanines did not promote structurally-pure enough aggregates, introducing different side chains on these compounds may lead to a more selective molecular packing. [71]

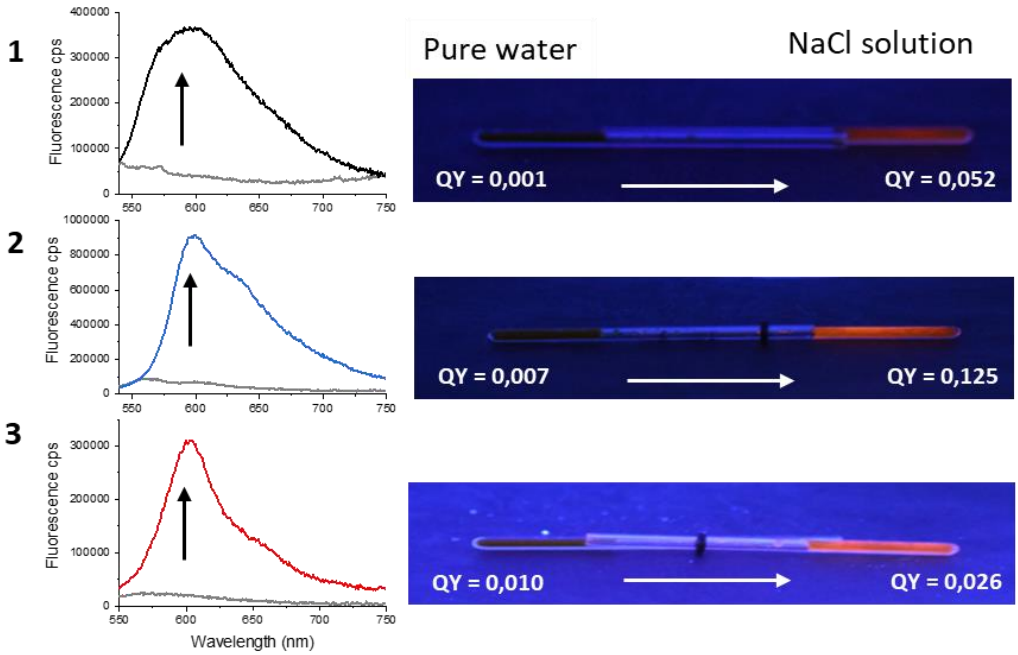

Fig. 11. Emission of **1**, **2** and **3** in pure water (grey) and in NaCl (3M) and corresponding photos of capillaries exposed to a 360 nm UV-lamp. Fluorescence quantum yield (QY) were estimated in an integrating sphere at 21 °C.

Aggregates spectra were then superimposed with fluorescence signal measured *in cellulo* (Fig. 12). The wavelength of the aggregates emission proved to be close to the emission observed "*in cellulo*" which supports the hypothesis of aggregates formation inside the mitochondria. In addition, emission spectra were also recorded for the solid powders of **1**, **2** and **3** and no detectable fluorescence was measured (Fig. S3) demonstrating that fluorescence arises from a the particular dye aggregation observed in NaCl solutions. Interestingly, methylated products **2** and **3** featured sharper emission than non-methylated **1**, as if aggregates formed with **1** were a mixture of both 1H and 2H tautomers.

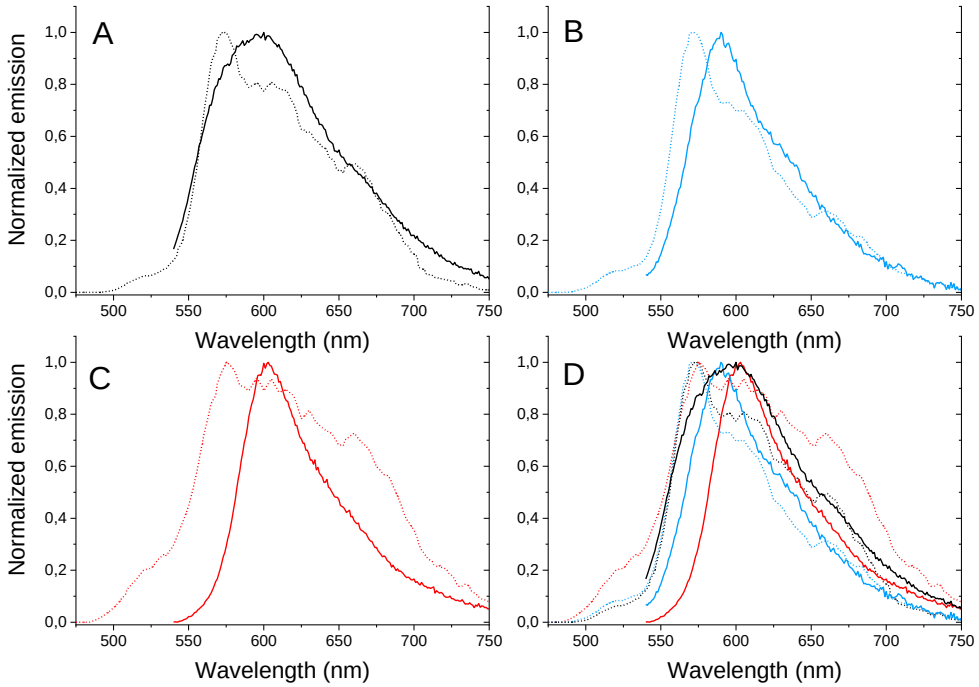

314

315 Fig. 12. Emission of aggregates (solid line) of **1** (A), **2** (B) and **3** (C) in a solution of NaCl (3M) and
316 superimposition (D) with *in cellulo* emission (dotted line).

317 The same experiments were carried out with indole compounds, fluorescence was detected upon
318 aggregation, but the intensity of this signal was very weak and no fluorescence quantum yield could
319 be measured. The emission of aggregates and *in cellulo* emission spectra did not superimpose,
320 suggesting that the emission of indole compounds **4** and **5** in cells is not related to an aggregation
321 effect (Fig. S4).

322 **3 Conclusion**

323 In this work, indazole was proposed for the first time as an electron-donating group to build cationic
324 merocyanine dyes. These molecules were easily synthesized and featured excellent ability to probe
325 viscosity in polar environment by comparison with commercial dyes. Their optical properties were
326 compared with those of indole merocyanines, and it appeared that indazoles are more pH sensitive,

and that a small modification such as methylation of nitrogen in position 2 can fundamentally change their optical properties allowing switching from push-pull to cyanine fluorophores.

Inside cells, indazoles compounds **1-3** provided selective fluorescence images of mitochondria as evidenced by co-labeling experiments. While an increased fluorescence was expected in mitochondria due to the viscosity of their membrane, indazole merocyanines also featured surprising red shifted excitation and emission spectra. This red shift is not correlated to viscosity, but probably results from the formation of J-aggregates inside of mitochondria as previously reported with other cationic dyes. To support the formation of this particular supra molecular arrangement, it was checked that these molecules feature no solid-state emission. However, it was not possible to fully demonstrate the formation of J-aggregates as the full widths at half maximum of emission spectra were too large, and we were unable to measure absorption spectra of these aggregates. This apparent red shift in mitochondria is very valuable for fluorescent imaging because it permits to trustworthy discriminate dyes inside the mitochondria from cytoplasmic dyes, and it shifts dyes absorption and emission closer to the biological transparency window.

4 Experimental section

4.1 Synthesis

Material and methods: Indole 99% was purchased from Acros Organics, and solvents from Fisher scientific. Column chromatography purifications were performed on silica gel (40–63 µm). Thin-layer chromatography (TLC) analyses were carried out on Merck DC Kieselgel 60 F-254 aluminum sheets. The spots were visualized through illumination with UV lamp (λ = 254 nm and 360 nm). IR spectra were recorded with a universal ATR sampling accessory. 1H and 13C NMR spectra (C13APT or C13CPD experiments) were recorded on a 300 MHz spectrometer. Chemical shifts are expressed in parts per

million (ppm) from the residual non-deuterated solvent signal contained in CDCl3 (δH = 7.26, δC = 77.16), in acetone-d6 (δH = 2.05, δC = 29.84) and in DMSO-d6 (δH = 2.50, δC = 39.52). Multiplicities are described as s (singlet), d (doublet), t (triplet), brs (broad peak) etc. Coupling constants, J values, are reported in Hz. High-resolution mass spectra (HRMS) were obtained using an orthogonal acceleration time-of-flight (oa-TOF) mass spectrometer equipped with an electrospray source and in the positive and negative modes (ESI+/−).

1*H*-indazole-3-carbaldehyde: The product was obtained following the protocol previously described by our team.[15]

To a solution of $NaNO_2$ (550 mg, 8 mmol, 8 eq.) in 4 mL of deionized water and 3 mL of DMF at 0 °C was added slowly HCl (1.33 mL of 2 N aq., 2.7 mmol, 2.7 eq.) and the resulting mixture was kept under argon for 10 min. A solution of indole (117 mg, 1 mmol, 1 eq.) in DMF (1 mL) was then added at 0 °C over a period of 2 h using a syringe pump. After addition, the reaction was stirred 3 additional hours at room temperature or until disappearance of intermediate products. The product was purified by column chromatography on silica gel, eluting with petroleum ether/EtOAc, 8 : 2 to provide the pure compound as a white solid (145 mg, 99%). Silica gel TLC Rf 0.37 (petroleum ether/EtOAc, 3 : 2); **^{1}H NMR ($SO(CD_3)_2$, 300 MHz):** δ (ppm) 14.17 (brs, 1H), 10.20 (s, 1H), 8.14 (d, *J* = 8.5 Hz, 1H), 7.70 (d, *J* = 8.5 Hz, 1H), 7.49 (dt, *J* = 7.0, 1.0 Hz, 1H), 7.37 (dt, *J* = 7.0, 1.0 Hz, 1H); **^{13}C NMR ($SO(CD_3)_2$, 75 MHz)** δ : 187.4, 143.4, 141.1, 127.3, 123.8, 120.7, 120.2, 111.2; **IR:** ν (cm^{-1}) = 3254, 3174, 1671, 1458, 1331, 1251, 1092, 792, 739; **HRMS (ESI^-):** found = 145.0402, $C_8H_5N_2O$ $[M-H]^-$ = 145.0390. **m.p.:** 141 °C.

1-methyl-1*H*-indazole-3-carbaldehyde 6: 1*H*-indazole-3-carbaldehyde (730 mg, 5 mmol) in dry MeCN (5 mL) was treated with iodomethane (0.50 mL, 1.5 eq.) in presence of K_2CO_3 (1.0 g, 1.5 eq.). The solution was refluxed for 16 h, then neutralized with a solution NH_4Cl and extracted 3 times with EtOAc. The crude mixture was composed of N_1 and N_2 methylated products with a ratio of 75:15 respectively

(determined by ^{1}H NMR spectroscopy). Both isomers were isolated by flash chromatography (cyclohexane: DCM: EtOAc 65:30:5) (464 mg, white amorphous solid, 58% isolated yield). **^{1}H NMR ($CDCl_3$, 300 MHz):** δ (ppm) = 10.23 (s, 1H), 8.31 (dt, 1H, *J* = 8.1, 1.0 Hz), 7.54 – 7.45 (m, 2H), 7.37 (m, 1H, *J* = 7.9, 5.5, 2.3 Hz), 4.20 (s, 3H). **^{13}C NMR ($CDCl_3$, 75 MHz):** δ (ppm) = 186.7, 143.1, 141.5, 127.6, 124.2, 122.4, 122.2, 109.5, 36.7. **IR:** ν (cm^{-1}) = 3059, 2949, 2792, 1671, 1474, 1426, 1254, 1060, 788, 749, 741. **HRMS (ESI^+):** found = 161.07159; calculated $[M+H]^+ = [C_9H_9N_2O]^+$= 161.07149. **m.p.:** 62-63 °C.

2-methyl-2*H*-indazole-3-carbaldehyde 7: See 1-methyl-1*H*-indazole-3-carbaldehyde (104 mg, white solid, 13% isolated yield). **^{1}H NMR ($CDCl_3$, 300 MHz):** δ (ppm) = 10.28 (s, 1H), 8.03 – 7.94 (m, 1H), 7.85 – 7.77 (m, 1H), 7.42 – 7.30 (m, 2H), 4.48 (s, 3H). **^{13}C NMR ($CDCl_3$, 75 MHz):** δ (ppm) = 177.5, 147.6, 130.5, 126.8, 126.4, 125.2, 118.7, 118.3, 40.9. **IR:** ν (cm^{-1}) = 2954, 2833, 1673, 1457, 1431, 1291, 1191, 1048, 780, 743. **HRMS (ESI^+):** found = 161.07128; calculated $[M+H]^+ = [C_9H_9N_2O]^+$= 161.07149. **m.p.:** 65-66 °C.

General procedure: (Knoevenagel condensation) Both the aldehyde (1 eq.) and 1-ethyl-3,3-dimethyl-3*H*-indolium iodide **4** (1 eq.) were solubilized in dry MeCN (final concentration of 1 M). Piperidine (10 mol%) was added and the solution was heated to 80 °C for 6 hours to 16 hours. The solvent was removed under reduced pressure and the crude mixture was purified by recrystallization in diethyl ether.

2-(2-(1*H*-indazol-3-yl)vinyl)-1-ethyl-3,3-dimethyl-3*H*-indolium iodide 1: The product was synthetized following the *general procedure* with 1*H*-indazole-3-carbaldehyde **5** (100 mg, 0.68 mmol) and 1-ethyl-2,3,3-trimethyl-3*H*-indolium iodide **4** (215 mg, 1 eq) (193 mg, pink solid, 64% isolated yield). **^{1}H NMR ($SO(CD_3)_2$, 300 MHz):** δ (ppm) = 14.43 (s, 1H), 8.67 (d, *J* = 16.3 Hz, 1H), 8.46 (d, *J* = 8.1 Hz, 1H), 8.03 –

7.89 (m, 2H), 7.80 – 7.60 (m, 4H), 7.56 (t, *J* = 7.7 Hz, 1H), 7.45 (t, *J* = 7.4 Hz, 1H), 4.73 (q, *J* = 7.0 Hz, 2H), 1.86 (s, 6H), 1.52 (t, *J* = 7.2 Hz, 3H). **^{13}C NMR ($SO(CD_3)_2$, 75 MHz):** δ (ppm) = 181.0, 144.0, 143.8, 141.7, 140.6, 140.5, 129.4, 129.2, 127.4, 123.5, 123.1, 122.4, 121.0, 115.1, 111.6, 111.3, 52.3, 42.2, 25.7, 13.5. **IR:** ν (cm^{-1}) = 3077, 3028, 2973, 1599, 1577, 1533, 1433, 1235, 1098, 958, 772, 748. **HRMS (ESI^+):** found = 316.1827; calculated $[M]^+$ = 316.1814. **m.p.:** 193-195 °C.

1-ethyl-3,3-dimethyl-2-(2-(1-methyl-1*H*-indazol-3-yl)vinyl)-3*H*-indolium iodide 2: The product was synthetized following the *general procedure* with 1-methyl-1*H*-indazole-3-carbaldehyde **6** (15 mg, 0.1 mmol) and 1-ethyl-2,3,3-trimethyl-3*H*-indolium iodide **4** (30 mg, 1 eq) (20 mg, dark pink solid, 44% isolated yield). **^{1}H NMR ($CDCl_3$, 300 MHz):** δ (ppm) = 8.45 (d, *J* = 16.2 Hz, 1H), 8.42 – 8.36 (m, 1H), 7.84 – 7.78 (m, 1H), 7.74 (d, *J* = 16.2 Hz, 1H), 7.65 – 7.53 (m, 6H), 5.01 (q, *J* = 7.4 Hz, 2H), 4.25 (s, 3H), 1.91 (s, 6H), 1.69 (t, *J* = 7.4 Hz, 3H). **^{13}C NMR ($CDCl_3$, 75 MHz):** δ (ppm) = 180.8, 144.8, 143.3, 142.0, 140.6, 139.9, 130.04, 130.00, 128.1, 125.4, 123.8, 122.83, 121.73, 115.4, 111.2, 110.5, 52.6, 44.9, 37.2, 27.2, 14.1. **IR:** ν (cm^{-1}) = 3003, 2976, 1592, 1534, 1455, 1311, 1237, 1065, 750. **HRMS (ESI^+):** found = 330.1975; calculated $[M]^+$ = 330.1970. **m.p.:** decomposition > 195 °C.

1-ethyl-3,3-dimethyl-2-(2-(2-methyl-2*H*-indazol-3-yl)vinyl)-3*H*-indolium iodide 3: The product was synthetized following the *general procedure* with 2-methyl-2*H*-indazole-3-carbaldehyde **7** (15 mg, 0.1 mmol) and 1-ethyl-2,3,3-trimethyl-3*H*-indolium iodide **4** (30 mg, 1 eq) (30 mg, dark purple solid, 66% isolated yield). **^{1}H NMR (CD_3OD, 300 MHz):** δ (ppm) = 8.55 – 8.46 (m, 1H), 8.27 – 8.21 (m, 1H), 7.92 – 7.85 (m, 2H), 7.85 – 7.80 (m, 1H), 7.71 – 7.63 (m, 2H), 7.59 – 7.51 (m, 3H), 4.75 (q, 2H, *J* = 7.3 Hz), 4.54 (s, 3H), 1.93 (s, 6H), 1.67 (t, 3H, *J* = 7.4 Hz). **^{13}C NMR (CD_3OD, 75 MHz):** δ (ppm) = 149.8, 145.2, 142.0, 138.41, 138.31, 132.6, 131.0, 130.8, 128.5, 128.3, 124.2, 124.1, 121.5, 120.3, 115.9, 111.2, 53.8, 43.6, 39.8, 26.9, 13.7. **IR:** ν (cm^{-1}) = 2976, 2932, 1582, 1569, 1427, 1290, 1243, 1065, 760. **HRMS (ESI^+):** found = 330.1964; calculated $[M]^+$ = 330.1970. **m.p.:** decomposition > 150 °C.

2-(2-(1H-indol-3-yl)vinyl)-1-ethyl-3,3-dimethyl-3H-indolium iodide 4: The product was synthetized following the *general procedure* with 1H-indole-3-carbaldehyde (145 mg, 1.0 mmol) and 1-ethyl-2,3,3-trimethyl-3H-indolium iodide (315 mg, 1 eq) (260 mg, pink solid, 59% isolated yield). **^{1}H NMR (CD_3OD, 300 MHz):** δ (ppm) =8.75 (d, 1H, *J* = 15.6 Hz), 8.49 (s, 1H), 8.13 (dd, 1H, *J* = 6.5, 1.8 Hz), 7.73 – 7.37 (m, 7H), 7.27 (d, 1H, *J* = 15.6 Hz), 4.56 (q, 2H, *J* = 7.3 Hz), 1.87 (s, 6H), 1.58 (t, 3H, *J* = 7.3 Hz). **^{13}C NMR (CD_3OD, 75 MHz):** δ (ppm) = 181.4, 151.3, 144.0, 142.2, 141.6, 140.4, 130.3, 129.0, 126.4, 126.0, 124.9, 123.9, 122.0, 118.0, 114.5, 114.2, 105.4, 52.6, 42.0, 27.5, 13.1. **IR:** ν (cm-1) = 3398, 3099, 2974, 1585, 1463, 1422, 1298, 1230, 1116, 748. **HRMS (ESI+):** $[M]^+$ found 315.1866; calculated for $[C22N23N2]^+$ 315.1861. **m.p.:** 68-69°C.

2-(2-(1methyl-indol-3-yl)vinyl)-1-ethyl-3,3-dimethyl-3H-indolium iodide 5: The product was synthetized following the *general procedure* with 1H-indole-3-carbaldehyde (145 mg, 1.0 mmol) and 1-ethyl-2,3,3-trimethyl-3H-indolium iodide (315 mg, 1 eq) (260 mg, pink solid, 59% isolated yield). **^{1}H NMR ($SO(CD_3)_2$, 300 MHz):** δ (ppm) = 8.77 (s, 1H), 8.69 (d, *J* = 15.7 Hz, 1H), 8.31 - 8.25 (m, 1H), 7.82 (d, *J* = 7.3 Hz, 1H), 7.77 (d, *J* = 7.7 Hz, 1H), 7.74 - 7.68 (m, 1H), 7.56 (td, J = 7.7 Hz, J = 1.8 Hz, 1H) , 7.51 (d, J = 7.7 Hz, 1H), 7.47 - 7,43 (m, 2H), 7.19 (d, *J* = 15.7 Hz, 1H), 4.57 (q, J = 7.2 Hz, 2H), 3.99 (s, 3H), 1.81 (s, 6H), 1.44 (t, *J* = 7.2 Hz, 3H).**^{13}C NMR ($SO(CD_3)_2$, 75 MHz):** δ (ppm) = 179.2, 148.5, 143.3, 142.7, 140.7, 139.0, 128.9, 127.5, 125.3, 124.5, 123.6, 122.9, 121.3, 114.9, 113.4, 112.1, 104.2, 50.9, 40.6, 34.1, 26.5, 12.8. **HRMS (ESI+):** $[M]^+$ found 329.2020; calculated for $[C23N25N2]^+$ 329.2018.

4.2 UV-visible spectroscopy

UV-visible absorption spectra were recorded with a Cary 60 (Agilent) applying a baseline correction. Steady state fluorescence was measured with a Horiba Fluorolog 3-21 (Hamamatsu photomultiplier tube R13456) using diluted samples O.D.< 0,1.

The dependence of fluorescence upon viscosity was measured by varying the temperature of an ethylene glycol solution from 10 °C to 60 °C.

Fluorescence quantum yields (ϕf) were measured thanks to the equation: ϕf = ϕfr x [F/Fr] x [(1-10^(-A)/(1-10^(-Ar)] x [n/nr]² were “F” is the integrated fluorescence signal of the dye, “Fr” is the integrated fluorescence signal of the reference; A and Ar the absorbance the dye and the reference respectively; n and nr the refractive index of the solvent dye and the solvent reference respectively.

Fluorescence lifetimes were measured by TCSPC using a delta diode 506 nm excitation source.

J-aggregates emission was measured in an integrating sphere G8 (General Microtechnology and Photonics) in a Horiba Fluorolog 3-21. J-aggregate were generated by introducing a solution of 10mg/ml of dye inside an integrating sphere capillary then adding the same amount of a saturated solution of NaCl (6M) or pure water for control experiments. The corrected spectra were measured and the blank signal was subtracted, taking into account the extinction caused by the sample. Quantum yields were calculated (excitation 520 nm) using the following equation: $\phi f = (f_p - f_s)/(F_l \times (l_s - l_p))$ were fp and fs are fluorescence signals (540 - 750nm) with and without product respectively F_l is the transmission of a 1% DO filter (Thorlabs) at excitation wavelength and l_p and l_s are lamp signal (510 – 530 nm) with and without product respectively.

3.3 Cell imaging

Cell Culture

As previously described (Raoult et al., 2011), tumoral PC12 cells, derived from a rat adrenal medulla pheochromocytoma, were cultured in a humidified incubator at 37 °C with an atmosphere of 5 % CO_2. Cells were grown in Dulbecco's modified Eagle's medium (DMEM) (Thermo Fisher Scientific, Illkirch, France) supplemented with 7 % heat-inactivated fetal bovine serum (Sigma–Aldrich), 7 % horse serum (Lonza Bioscience, Walkersville, MD, USA), 2.5 % HEPES (4-(2-hydroxyethyl)-1-piperazine

ethanesulfonic acid) (Thermo Fisher Scientific), 1 % glutamine (Thermo Fisher Scientific), 100 units/mL penicillin and 100 µg mL^{-1} streptomycin (Thermo Fisher Scientific).

Cytotoxicity assay

PC12 cells were prepared for cell viability studies in 24-well plates (ThermoFisher Scientific, Montigny le Bretonneux, France). The cells were incubated for 1 or 24 hours with a single merocyanine compound (**1**, **2** or **3**) at a concentration of 10^{-6} M. Two drops of NucGreenTM Dead 488 ReadyProbes reagent (Thermo Fisher Scientific) per mL of media to test indazole compounds **1**, **2** or **3**, and 2µM of Ethidium Homodimer (Exc 633nm; Invitrogen) to test **4** and **5** indole compounds (B) were added into wells, followed by further incubation for 10 min at 37 °C. Since the NucGreen and Ethidium are cell-impermeant and emits green fluorescence when bound to DNA, the viability was determined by imaging, through transmitted and fluorescence modes, positive cells on an automated boxed inverted Zeiss CD7 microscope piloted with Zen software (Carl Zeiss, Jena, Germany). Statistical analysis was performed with the GraphPad Prism 4 software (GraphPad Software Inc.) and a one-way Analysis of Variance (ANOVA) with a Tukey-Kramer multiple comparisons tests was used.

Cell labelling

For fluorescent labelling with merocyanine compounds, PC12 cells were plated on glass bottom dishes (grade 1.5 MatTek Corporation, MA, USA) and culture for 1 day. Prior dilution in phenol red-free Dulbecco's modified Eagle's medium (DMEM), solubilization of compounds was facilitated with the non-ionic surfactant polyol Pluronic F-127 (ThermoFisher Scientific) (v/v). For live cell imaging, cells were incubated with indazole and indole merocyanine dyes (final concentration: 10^{-6} M) during 45 min, rinsed once and observed.

Confocal microscopy

Emission/excitation spectra of indazole and indole merocyanine dyes from labelled cells

1-photon excitation and emission spectra were measured using λΔ acquisition mode on an inverted Leica TCS SP5 confocal microscope (Leica Microsystems, Nanterre, France) equipped with a supercontinuum laser source (NTK photonics, Cologne, Germany) and a resonant scanner (8000 Hz). Using a 20x objective (0.70, oil immersion), fluorescence emission from labelled living cells was detected through a hybrid detector (HyD) in the counting mode (Leica Micro-systems, France). In this configuration, two-dimensional scanning with automatic variations of excitation (Δ from 470 to 670 nm, 2 nm step) and emission (λ, from 480 to 795 nm, 10 nm band) was performed and led to a stack of 1722 images (n=6). Resulting λΔ representation and excitation/emission spectra were obtained using the Excitation Emission Contour Plot of the Leica Application Suite Advanced Fluorescence software (Leica Microsystems, France).

Subcellular localization of merocyanine dyes in living cells

Subcellular imaging was performed on an inverted Leica TCS SP5 confocal microscope equipped with a supercontinuum laser source and a conventionnal scanner (400 Hz). In phenol red-free DMEM, **1**, **2** or **3** indazole merocyanines were excited at 543 nm and fluorescence was collected with a HyD (photon counting mode) from 560 to 620 nm; **4** or **5** indole merocyanines were excited at 488 nm. A 63x objective (NA 1.4) and an optical zoom factor of 2.5 were used and z-stacks parameters (z-step = 250 nm; z-stack= between 4 to 6 µm) were set. For mitochondria labeling, incubation with Mitotracker Green TM (Thermo Fisher Scientific) at a concentration of 500 nM during 30 min was performed following staining with indazole compounds **1**, **2** or **3**. For indole compounds **4** and **5**, Mitotracker Red TM (Thermo Fisher Scientific) was used. For cell imaging, Mitotracker Green was excited at 488 nm and fluorescence was collected from 500 to 540 nm, and Mitotracker Red was excited at 594 nm and fluorescence collected from 605 to 665 nm. All double labeling experiments were performed through a sequential mode of acquisition to avoid any spectral contamination.

Image Analysis

To improve signal-to-noise ratio in confocal images, deconvolution of raw data was obtained through image processing with Huygens professional 4.5.1 software (SVI, The Netherlands). ImageJ (Rasband, W.S., U. S. National Institutes of Health, Bethesda, Maryland, USA, http://imagej.nih.gov/ij/, 1997-2016) was used to adjust image brightness and contrast and to perform projections of 3D images (xyz).

CRediT authorship contribution statement

Margot Boujut: Investigation ; **Arnaud Chevalier :** Conceptualization, Investigation, Writing - Review & Editing ; **Damien Schapman:** Investigation; **Magalie Bénard:** Investigation; **Ludovic Galas:** Writing - Original Draft, Visualization, Project administration, Funding acquisition ; **Thibault Gallavardin:** Conceptualization, Investigation, Writing - Original Draft, Project, administration, Funding acquisition ; **Xavier Franck :** Writing - Review & Editing, Project administration, Funding acquisition

Acknowledgements

This work has been partially supported by University of Rouen Normandy, the Centre National de la Recherche Scientifique (CNRS), INSA Rouen Normandy, European Regional Development Fund (FEDER HN0005444 - E2M2, and FEDER HN0001401-Chimbio - COMUE Normandie Université), Labex SynOrg (ANR-11-LABX-0029), Carnot Institute I2C, The French ANR JCJC 2019 program (ANR-19-CE18-0006), (the graduate school for research XL-Chem (ANR-18-EURE-0020 XL CHEM)), and by Region Normandie. We are grateful to Alexandre Arnaud, Claire Desjardin for synthesis, Patricia Martel (University of Rouen Normandy) for IR analyses, and to Albert Marcual (CNRS) for HRMS analyses.

[1] Wang W, Liu Y, Niu J, Lin W. Discriminating normal and inflammatory models by viscosity changes with a mitochondria-targetable fluorescent probe. Analyst 2019;144:6247–53. https://doi.org/10.1039/C9AN01573F.

[2] Conradt B. Mitochondria Shape Up. Nature 2006;443:646–647. https://doi.org/10.1038/443646a.

[3] Chan DC. Mitochondria: Dynamic Organelles in Disease, Aging, and Development. Cell 2006;125:1241–52. https://doi.org/10.1016/j.cell.2006.06.010.

[4] Smith RAJ, Porteous CM, Gane AM, Murphy MP. Delivery of bioactive molecules to mitochondria in vivo. Proc Natl Acad Sci 2003;100:5407–12. https://doi.org/10.1073/pnas.0931245100.

[5] Murphy MP. Selective targeting of bioactive compounds to mitochondria. Trends Biotechnol 1997;15:326–30. https://doi.org/10.1016/S0167-7799(97)01068-8.

[6] Lee D, Jung M-K, Yin J, Kim G, Pack C-G, Yoon J. An aniline bearing hemicyanine derivative serves as a mitochondria selective probe. Dyes Pigments 2017;136:467–72. https://doi.org/10.1016/j.dyepig.2016.09.010.

[7] Xiao H, Dong Y, Zhou J, Zhou Z, Wu X, Wang R, Miao Z, Liu Y, Zhuo S. Monitoring Mitochondrial pH with a Hemicyanine-Based Ratiometric Fluorescent Probe. Analyst 2019;144:3422–3427. https://doi.org/10.1039/C9AN00422J.

[8] Zhang Y, Xia S, Mikesell L, Whisman N, Fang M, Steenwinkel TE, Chen K, Luck RL, Werner T, Liu H. Near-Infrared Hybrid Rhodol Dyes with Spiropyran Switches for Sensitive Ratiometric Sensing of pH Changes in Mitochondria and Drosophila Melanogaster First-Instar Larvae. ACS Appl. Bio Mater. 2019;2:4986–4997. https://doi.org/10.1021/acsabm.9b00710.

[9] Chen Y, Zhu C, Cen J, Bai Y, He W, Guo Z. Ratiometric Detection of PH Fluctuation in Mitochondria with a New Fluorescein/Cyanine Hybrid Sensor. Chem. Sci. 2015;6:3187–3194. https://doi.org/10.1039/C4SC04021J.

[10] Yang XZ, Xu B, Shen L, Sun R, Xu YJ, Song YL, Ge JF. Series of Mitochondria/Lysosomes Self-Targetable Near-Infrared Hemicyanine Dyes for Viscosity Detection. Anal. Chem. 2020;92: 3517–3521. https://doi.org/10.1021/acs.analchem.0c00054.

[11] Li, X.; Hu, Y.; Li, X.; Ma, H. Mitochondria-Immobilized Near-Infrared Ratiometric Fluorescent PH Probe To Evaluate Cellular Mitophagy. Anal. Chem. 2019;91:11409–11416. https://doi.org/10.1021/acs.analchem.9b02782.

[12] Roopa, Kumar N, Bhalla V, Kumar M. Development and Sensing Applications of Fluorescent Motifs within the Mitochondrial Environment. Chem. Commun. 2015;51:15614–15628. https://doi.org/10.1039/C5CC07098H.

[13] Zhang L, Liu W, Huang X, Zhang G, Wang X, Wang Z, Zhang D, Jiang X. Old Is New Again: A Chemical Probe for Targeting Mitochondria and Monitoring Mitochondrial Membrane Potential in Cells. Analyst 2015;140:5849–5854. https://doi.org/10.1039/C5AN00918A.

[14] Yin J, Peng M, Lin W. Visualization of Mitochondrial Viscosity in Inflammation, Fatty Liver, and Cancer Living Mice by a Robust Fluorescent Probe. Anal. Chem. 2019;91:8415–8421. https://doi.org/10.1021/acs.analchem.9b01293.

[15] Jakobs S. High Resolution Imaging of Live Mitochondria. Biochim. Biophys. Acta BBA - Mol. Cell Res. 2006, 1763 (5), 561–575. https://doi.org/10.1016/j.bbamcr.2006.04.004.

[16] Baek Y, Park SJ, Zhou X, Kim G, Kim HM, Yoon J. A Viscosity Sensitive Fluorescent Dye for Real-Time Monitoring of Mitochondria Transport in Neurons. Biosens. Bioelectron 2016;86:885–891. https://doi.org/10.1016/j.bios.2016.07.026.

[17] Chen B, Gong W, Yang Z, Pan W, Verwilst P, Shin J, Yan W, Liu L, Qu J, Kim JS. STORM Imaging of Mitochondrial Dynamics Using a Vicinal-Dithiol-Proteins-Targeted Probe. Biomaterials 2020; 243:119938. https://doi.org/10.1016/j.biomaterials.2020.119938.

[18] Zheng A, Liu H, Gao X, Xu K, Tang B. A Mitochondrial-Targeting Near-Infrared Fluorescent Probe for Revealing the Effects of Hydrogen Peroxide And Heavy Metal Ions on Viscosity. Anal. Chem. 2021;93:9244–9249. https://doi.org/10.1021/acs.analchem.1c01511.

[19] Zou Z, Yan Q, Ai S, Qi, P, Yang H, Zhang Y, Qing Z, Zhang L, Feng F, Yang R. Real-Time Visualizing Mitophagy-Specific Viscosity Dynamic by Mitochondria-Anchored Molecular Rotor. Anal. Chem. 2019;91:8574–8581. https://doi.org/10.1021/acs.analchem.9b01861.

[20] Rimpelová S, Bříza T, Králová J, Záruba K, Kejík Z, Císařová I, Martásek P, Ruml T, Král V. Rational Design of Chemical Ligands for Selective Mitochondrial Targeting. Bioconjug. Chem. 2013;24:1445–1454. https://doi.org/10.1021/bc400291f.

[21] Yang Z, He Y, Lee JH, Park N, Suh M, Chae WS, Cao J, Peng X, Jung H, Kang C, Kim JS. A Self-Calibrating Bipartite Viscosity Sensor for Mitochondria. J. Am. Chem. Soc. 2013;135:9181–9185. https://doi.org/10.1021/ja403851p.

[22] Du Y, Wang H, Zhang T, Wei W, Guo M. ICT-Based Fluorescent Ratiometric Probe for Monitoring Mitochondrial Peroxynitrite in Living Cells. New J. Chem. 2021;45:12915–12921. https://doi.org/10.1039/D1NJ01713F.

[23] Wang C, Wang T, Zhao M, Dai F, Niu Z, Zhang W, Ma Y. A Simple Chalcone Molecular Rotor for Specific Fluorescence Imaging of Mitochondrial Viscosity Changes in Living Cells. Dyes Pigments 2021;194:109593. https://doi.org/10.1016/j.dyepig.2021.109593.

[24] Yin X, Cai Y, Cai S, Jiao X, Liu C, He S, Zeng X. A Deep-Red Fluorescent Molecular Rotor Based on Donor-Two-Acceptor Modular System for Imaging Mitochondrial Viscosity. RSC Adv. 2020;10: 30825–30831. https://doi.org/10.1039/D0RA04935B.

[25] Modica-Napolitano JS, Aprille JR. Delocalized Lipophilic Cations Selectively Target the Mitochondria of Carcinoma Cells. Adv. Drug Deliv. Rev. 2001;49:63–70. https://doi.org/10.1016/S0169-409X(01)00125-9.

[26] Wu Y, Shu W, Zeng C, Guo B, Shi J, Jing J, Zhang X. A Mitochondria Targetable and Viscosity Sensitive Fluorescent Probe and Its Applications for Distinguishing Cancerous Cells. Dyes Pigments 2019; 168:134–139. https://doi.org/10.1016/j.dyepig.2019.04.049.

[27] Ruiz-González R, Acedo P, Sánchez-García D, Nonell S, Cañete M, Stockert JC, Villanueva A. Efficient Induction of Apoptosis in HeLa Cells by a Novel Cationic Porphycene Photosensitizer. Eur. J. Med. Chem. 2013;63:401–414. https://doi.org/10.1016/j.ejmech.2013.02.028.

[28] Morgan J, Oseroff AR. Mitochondria-Based Photodynamic Anti-Cancer Therapy. Adv. Drug Deliv. Rev. 2001;49:71–86. https://doi.org/10.1016/S0169-409X(01)00126-0.

[29] Bunting JR. A Test of the Singlet Oxygen Mechanism of Cationic Dye Photosensitization of Mitochondrial Damage. Photochem. Photobiol. 1992;55:81–87. https://doi.org/10.1111/j.1751-1097.1992.tb04212.x.

[30] Celli JP, Spring BQ, Rizvi I, Evans CL, Samkoe KS, Verma S, Pogue B W, Hasan T. Imaging and Photodynamic Therapy: Mechanisms, Monitoring, and Optimization. Chem. Rev. 2010;110: 2795–2838. https://doi.org/10.1021/cr900300p.

[31] Zielonka J, Joseph J, Sikora A, Hardy M, Ouari O, Vasquez-Vivar J, Cheng G, Lopez M, Kalyanaraman B. Mitochondria-Targeted Triphenylphosphonium-Based Compounds: Syntheses,

Mechanisms of Action, and Therapeutic and Diagnostic Applications. Chem. Rev. 2017;117:10043–10120. https://doi.org/10.1021/acs.chemrev.7b00042.

[32] Qian K, Chen H, Qu C, Qi J, Du B, Ko T, Xiang Z, Kandawa-Schulz M, Wang Y, Cheng Z. Mitochondria-Targeted Delocalized Lipophilic Cation Complexed with Human Serum Albumin for Tumor Cell Imaging and Treatment. Nanomedicine Nanotechnol. Biol. Med. 2020;23:102087. https://doi.org/10.1016/j.nano.2019.102087.

[33] Chen H, Wang J, Feng X, Zhu M, Hoffmann S, Hsu A, Qian K, Huang D, Zhao F, Liu W, Zhang H, Cheng Z. Mitochondria-Targeting Fluorescent Molecules for High Efficiency Cancer Growth Inhibition and Imaging. Chem. Sci. 2019;10:7946–7951. https://doi.org/10.1039/C9SC01410A.

[34] Zhou K, Ren M, Deng B, Lin W. Development of a Viscosity Sensitive Fluorescent Probe for Real-Time Monitoring of Mitochondria Viscosity. New J. Chem. 2017;41:11507–11511. https://doi.org/10.1039/C7NJ02270K.

[35] Gong J, Liu C, Jiao X, He S, Zhao L, Zeng X. Novel Mitochondria-Targeted Viscosity Probe Based on a Fluorescent Rotatable Xanthene-Hemicyanine Dyad. Microchem. J. 2020;158:105191. https://doi.org/10.1016/j.microc.2020.105191.

[36] Zhang Y, Li Z, Hu W, Liu Z. A Mitochondrial-Targeting Near-Infrared Fluorescent Probe for Visualizing and Monitoring Viscosity in Live Cells and Tissues. Anal. Chem. 2019;91:10302–10309. https://doi.org/10.1021/acs.analchem.9b02678.

[37] Park SJ, Shin BK, Lee HW, Song JM, Je JT, Kim HM. Asymmetric Cyanine as a Far-Red Fluorescence Probe for Mitochondrial Viscosity. Dyes Pigments 2020;174:108080. https://doi.org/10.1016/j.dyepig.2019.108080.

[38] Zhang R, Niu G, Li X, Guo L, Zhang H, Yang R, Chen Y, Yu X, Tang BZ. Reaction-Free and MMP-Independent Fluorescent Probes for Long-Term Mitochondria Visualization and Tracking. Chem. Sci. 2019;10:1994–2000. https://doi.org/10.1039/C8SC05119D.

[39] Sampson PB, Liu Y, Patel NK, Feher M, Forrest B, Li SW, Edwards L, Laufer R, Lang Y, Ban F, Awrey DE, Mao G, Plotnikova O, Leung G, Hodgson R, Mason J, Wei X, Kiarash R, Green E, Qiu W, Chirgadze NY, Mak TW, Pan G, Pauls HW. The Discovery of Polo-Like Kinase 4 Inhibitors: Design and Optimization of Spiro[Cyclopropane-1,3′[3 H]Indol]-2′(1′ H)-Ones as Orally Bioavailable Antitumor Agents. J. Med. Chem. 2015;58:130–146. https://doi.org/10.1021/jm500537u.

[40] Laufer R, Forrest B, Li SW, Liu Y, Sampson P, Edwards L, Lang Y, Awrey DE, Mao G, Plotnikova O, Leung G, Hodgson R, Beletskaya I, Mason JM, Luo X, Wei X, Yao Y, Feher M, Ban F, Kiarash R Green E, Mak, T W, Pan G, Pauls HW. The Discovery of PLK4 Inhibitors: (E)-3-((1 H -Indazol-6-Yl)Methylene)Indolin-2-Ones as Novel Antiproliferative Agents. J. Med. Chem. 2013;56:6069–6087. https://doi.org/10.1021/jm400380m.

[41] McBride CM, Renhowe PA, Gesner TG, Jansen JM, Lin J, Ma S, Zhou Y, Shafer CM. 3-Benzimidazol-2-Yl-1H-Indazoles as Potent c-ABL Inhibitors. Bioorg. Med. Chem. Lett. 2006;16:3789–3792. https://doi.org/10.1016/j.bmcl.2006.04.043.

[42] Zhao G, Li W, Chen D, Henry JR, Li HY, Chen Z, Zia-Ebrahimi M, Bloem L, Zhai Y, Huss K, Peng SB, McCann DJ. A Novel, Selective Inhibitor of Fibroblast Growth Factor Receptors That Shows a Potent Broad Spectrum of Antitumor Activity in Several Tumor Xenograft Models. Mol. Cancer Ther. 2011;10:2200–2210. https://doi.org/10.1158/1535-7163.MCT-11-0306.

[43] Angelova, V. T.; Pencheva, T.; Vassilev, N.; Simeonova, R.; Momekov, G.; Valcheva, V. New Indole and Indazole Derivatives as Potential Antimycobacterial Agents. *Med. Chem. Res.* **2019**, *28* (4), 485–497. https://doi.org/10.1007/s00044-019-02293-w.

[44] McTigue M, Murray BW, Chen JH, Deng YL, Solowiej J, Kania RS. Molecular Conformations, Interactions, and Properties Associated with Drug Efficiency and Clinical Performance among VEGFR TK Inhibitors. Proc. Natl. Acad. Sci. 2012;109:18281–18289. https://doi.org/10.1073/pnas.1207759109.

[45] Lower SK, El-Sayed MA. The Triplet State and Molecular Electronic Processes in Organic Molecules. Chem. Rev. 1966;66:199–241. https://doi.org/10.1021/cr60240a004.

[46] Chipem FAS, Mishra A, Krishnamoorthy G. The Role of Hydrogen Bonding in Excited State Intramolecular Charge Transfer. Phys. Chem. Chem. Phys. 2012;14:8775–8790. https://doi.org/10.1039/C2CP23879A.

[47] Catalan J, del Valle JC, Claramunt RM, Boyer G, Laynez J, Gomez J, Jimenez P, Tomas F, Elguero J. Acidity and Basicity of Indazole and Its N-Methyl Derivatives in the Ground and in the Excited State. J. Phys. Chem. 1994;98:10606–10612. https://doi.org/10.1021/j100092a035.

[48] Chevalier A, Ouahrouch A, Arnaud A, Gallavardin T, Franck X. An Optimized Procedure for Direct Access to 1 H -Indazole-3-Carboxaldehyde Derivatives by Nitrosation of Indoles. RSC Adv. 2018; 8:13121–13128. https://doi.org/10.1039/C8RA01546E.

[49] Slade DJ, Pelz NF, Bodnar W, Lampe JW, Watson PS. Indazoles: Regioselective Protection and Subsequent Amine Coupling Reactions. J. Org. Chem. 2009;74:6331–6334. https://doi.org/10.1021/jo9006656.

[50] Ley C, Bordat P, di Stefano LH, Remongin L, Ibrahim A, Jacques P, Allonas X. Joint Spectroscopic and Theoretical Investigation of Cationic Cyanine Dye Astrazon Orange-R: Solvent Viscosity Controlled Relaxation of Excited States. Phys. Chem. Chem. Phys. 2015;17:5982–5990. https://doi.org/10.1039/C4CP05103C.

[51] Bar-On ZE, Iron MA, Kasdan HL, Amir D, Afrimzon E, Zurgil N, Moshkov S, Deutsch M. The Cationic Dye Basic Orange 21 (BO21) as a Potential Fluorescent Sensor. Photochem. Photobiol. Sci. 2018;17:1417–1428. https://doi.org/10.1039/C7PP00455A.

[52] Han WG, Lovell T, Liu T, Noodleman L. Density Functional Studies of the Ground- and Excited-State Potential-Energy Curves of Stilbenecis-Trans Isomerization. ChemPhysChem 2002;3:167–178. https://doi.org/10.1002/1439-7641(20020215)3:2<167::AID-CPHC167>3.0.CO;2-G.

[53] Würthner F, Wortmann R, Matschiner R, Lukaszuk K, Meerholz K, DeNardin Y, Bittner R, Bräuchle C, Sens R. Merocyanine Dyes in the Cyanine Limit: A New Class of Chromophores for Photorefractive Materials. Angew. Chem. Int. Ed. Engl. 1997;36:2765–2768. https://doi.org/10.1002/anie.199727651.

[54] Dragan A, Graham AE, Geddes CD. Fluorescence-Based Broad Dynamic Range Viscosity Probes. J. Fluoresc. 2014;24:397–402. https://doi.org/10.1007/s10895-013-1304-9.

[55] Zhu L, Fu M, Yin B, Wang L, Chen Y, Zhu Q. A Red-Emitting Fluorescent Probe for Mitochondria-Target Microviscosity in Living Cells and Blood Viscosity Detection in Hyperglycemia Mice. Dyes Pigments 2020;172:107859. https://doi.org/10.1016/j.dyepig.2019.107859.

[56] Rurack K, Spieles M. Fluorescence Quantum Yields of a Series of Red and Near-Infrared Dyes Emitting at 600−1000 Nm. Anal. Chem. 2011;83:1232–1242. https://doi.org/10.1021/ac101329h.

[57] Nani RR, Kelley JA, Ivanic J, Schnermann MJ. Reactive Species Involved in the Regioselective Photooxidation of Heptamethine Cyanines. Chem. Sci. 2015;6:6556–6563. https://doi.org/10.1039/C5SC02396C.

[58] Chung AJ, Deore PS, Al-Abdul-Wahid S, Aboelnga MM, Wetmore SD, Manderville RA. Acceptor Influence on Thiolate Sensing by Hemicyanine Dyes. J. Org. Chem. 2019;84:2261–2268 https://doi.org/10.1021/acs.joc.9b00066.

[59] Strekowski L, MasonJC, Britton JE, Lee H, Van Aken K, Patonay G. The Addition Reaction of Hydroxide or Ethoxide Ion with Benzindolium Heptamethine Cyanine Dyes. Dyes Pigments 2000;46:163–168. https://doi.org/10.1016/S0143-7208(00)00046-2.

[60] Li J, Chang Z, Pan X, Dong W, Jia AQ. A Novel Colorimetric and Fluorescent Probe Based on Indolium Salt for Detection of Cyanide in 100% Aqueous Solution. Dyes Pigments 2019;168: 175–179. https://doi.org/10.1016/j.dyepig.2019.04.059.

[61] Promchat A, Rashatasakhon P, Sukwattanasinitt M. A Novel Indolium Salt as a Highly Sensitive and Selective Fluorescent Sensor for Cyanide Detection in Water. J. Hazard. Mater. 2017;329: 255–261. https://doi.org/10.1016/j.jhazmat.2017.01.024.

[62] Xiong K, Huo F, Yin C, Yang Y, Chao J, Zhang Y, Xu M. A off–on Green Fluorescent Chemosensor for Cyanide Based on a Hybrid Coumarin–Hemicyanine Dye and Its Bioimaging. Sens. Actuators B Chem. 2015;220:822–828. https://doi.org/10.1016/j.snb.2015.05.084.

[63] Zhang Y, Yu D, Feng G. Colorimetric and near Infrared Fluorescent Detection of Cyanide by a New Phenanthroimidazole–Indolium Conjugated Probe. RSC Adv. 2014;4:14752–14757. https://doi.org/10.1039/C4RA00206G.

[64] Shiraishi Y, Nakamura M, Yamamoto K, Hirai T. Rapid, Selective, and Sensitive Fluorometric Detection of Cyanide Anions in Aqueous Media by Cyanine Dyes with Indolium–Coumarin Linkages. Chem. Commun. 2014;50:11583–11586. https://doi.org/10.1039/C4CC05412A.

[65] Lv X, Liu J, Liu Y, Zhao Y, Sun YQ, Wang P, Guo W. Ratiometric Fluorescence Detection of Cyanide Based on a Hybrid Coumarin –Hemicyanine Dye: The Large Emission Shift and the High Selectivity. Chem. Commun. 2011;47:12843–12845. https://doi.org/10.1039/C1CC15721C.

[66] Li L, Zhang Y, Chang Z, Bai FQ, Zhang HX, Ferri JK, Dong WF. Theoretical Study on Fluorescent Probes for Cyanide Based on the Indolium Functional Group. Org. Electron. 2016;30:1–11. https://doi.org/10.1016/j.orgel.2015.12.002.

[67] Würthner F, Kaiser TE, Saha-Möller CR. J-Aggregates: From Serendipitous Discovery to Supramolecular Engineering of Functional Dye Materials. Angew. Chem. Int. Ed. 2011;50:3376–3410. https://doi.org/10.1002/anie.201002307.

[68] Bricks JL, Slominskii YL, Panas ID, Demchenko AP Fluorescent J-Aggregates of Cyanine Dyes: Basic Research and Applications Review. Methods Appl. Fluoresc. 2017;6:012001. https://doi.org/10.1088/2050-6120/aa8d0d.

[69] Guralchuk GY, Katrunov IK, Grynyov RS, Sorokin AV, Yefimova SL, Borovoy IA, Malyukin YV. Anomalous Surfactant-Induced Enhancement of Luminescence Quantum Yield of Cyanine Dye J-Aggregates. J. Phys. Chem. C 2008;112:14762–14768. https://doi.org/10.1021/jp802933n.

[70] Smiley ST, Reers M, Mottola-Hartshorn C, Lin M, Chen A, Smith TW, Steele GD, Chen LB. Intracellular Heterogeneity in Mitochondrial Membrane Potentials Revealed by a J-Aggregate-Forming Lipophilic Cation JC-1. Proc. Natl. Acad. Sci. 1991;88:3671–3675. https://doi.org/10.1073/pnas.88.9.3671.

[71] Liess A, Lv A, Arjona-Esteban A, Bialas D, Krause AM, Stepanenko V, Stolte M, Würthner F. Exciton Coupling of Merocyanine Dyes from H- to J-Type in the Solid State by Crystal Engineering. Nano Lett. 2017;17 :1719–1726. https://doi.org/10.1021/acs.nanolett.6b0499

Graphical abstract